Modulating the Biological Function of Protein by Tailoring the Adsorption Orientation on Nanoparticles

*Akhil Jain, Gustavo F. Trindade, Jacqueline M. Hicks, Jordan C. Potts, Ruman Rahman, Richard J. M. Hague, David B. Amabilino, Lluïsa Pérez-García, and Frankie J. Rawson**

Dr. Akhil Jain, Dr. Jacqueline M. Hicks, Dr. Frankie J. Rawson*
Division of Regenerative Medicine and Cellular Therapies
School of Pharmacy, University of Nottingham
Nottingham NG7 2RD, UK
*E-mail: Frankie.Rawson@nottingham.ac.uk

Dr. Gustavo F. Trindade, Jordan C. Potts and Dr. Lluïsa Pérez-García
Division of Advanced Materials and Healthcare Technologies
School of Pharmacy, University of Nottingham
Nottingham NG7 2RD, UK

Dr. Ruman Rahman
Children's Brain Tumour Research Centre
School of Medicine, University of Nottingham
Nottingham NG7 2UH, UK

Prof. Richard J. M. Hague
Centre for Additive Manufacturing
Faculty of Engineering, University of Nottingham
Nottingham NG8 1BB, UK

Prof. David B. Amabilino
GSK Carbon Neutral Laboratories for Sustainable Chemistry
School of Chemistry, University of Nottingham
Nottingham NG7 2TU, UK

Abstract

Protein orientation in nanoparticle-protein conjugates plays a crucial role in binding to cell receptors and ultimately, defines their targeting efficiency. Therefore, understanding fundamental aspects of the role of protein orientation upon adsorption on the surface of nanoparticles (NPs) is vital for the development of clinically important protein-based nanomedicine. In this work, new insights on the effect of the different orientation of cytochrome *c* (cyt *c*) bound to gold nanoparticles (GNPs) using various ligands on its apoptotic activity is reported. Time-of-Flight Secondary-Ion Mass Spectrometry (ToF-SIMS), electrochemical and circular dichroism (CD) analyses are used to investigate the characteristics of cyt *c* orientation and structure on functionalized GNPs. These studies indicate that the orientation and position of the heme ring inside the cyt *c* structure can be altered by changing the surface chemistry on the NPs. A difference in the apoptosis inducing capability because of different orientation of cyt *c* bound to the GNPs is observed. These findings indicate that the biological activity of a protein can be modulated on the surface of NPs by varying its adsorption orientation. This study will impact on the rational design of new nanoscale biosensors, bioelectronics, and nanoparticle-protein based drugs.

Keywords: gold nanoparticles, cytochrome *c*, orientation, apoptosis, peroxidase activity

1. Introduction

Our ability to tailor surfaces at the nanoscale for biomedical and biotechnological applications is expanding at an ever-greater pace.[1-3] A key component of this field is the development of protein functionalized NPs.[4] The advancement of NP-protein conjugates for sensing, imaging, drug delivery and targeting is of interest for many diverse applications.[5-11] In particular, the NP-protein conjugates are regarded as new innovative therapeutic agents.[12-14] Upon conjugation to NPs, therapeutic proteins can be delivered specifically at a desired targeted site.[15, 16] One such protein is cyt *c*, that has attracted special attention because of its dual

role as an electron carrier in mitochondrial electron transfer chain (ETC) and as an initiator of apoptosis.[17, 18] Both these properties of cyt *c* arise from the presence of a redox-active heme moiety embedded in its structure.[19] Under apoptotic stimuli, cyt *c* translocate to the cytosol by gaining peroxidase activity thus causing the oxidation of Fe^{2+} (inactive form) of the heme moiety to Fe^{3+} (active form).[20] Upon reaching the cytosol this activated form of cyt *c* triggers the apoptosis cascade.[17] Therefore, in tumor cells where apoptosis rarely occurs (a hallmark of cancer), introduction of cyt *c* could initiate the destruction of malignant cells.[21] However, intracellular delivery of cyt *c* is challenging because of its size (~3.1 nm) and non-lipophilic nature.[22, 23] In order to address this delivery issue, mesoporous silica, lipid and hybrid NPs have been explored as delivery vehicles to enhance intracellular transport of cyt *c*.[24-26] There is however a lack of understanding on how to control and manipulate the protein structure and its orientation-dependent properties to tailor the biological effects of NP-protein conjugates. Therefore, conceptualizing the fundamental aspects of cyt *c* adsorption on NPs is important for predicting the impact of NP- cyt *c* conjugates on biological process, such as apoptosis.

The physicochemical properties of NPs have been shown to distort protein tertiary structure, which can perturb protein function.[27-30] To this end, studies have been conducted to identify the labelling/ binding site of the cyt *c* on NPs.[31, 32] Other factors such as NP size and charge have been identified to influence the structure of cyt *c* and thus its electron transfer and peroxidase activity.[33, 34] Protein orientation has also been shown to play a crucial role in its targeting ability.[35-41] However, in the case of cyt *c*, most of the investigations on determining its orientation have been limited to macro-sized flat surfaces rather than curved NP surfaces bearing different charge, which hinders its application at a cellular level.[42-49] Recently, Tollefson et al. inferred the orientation of cyt *c* on anionic ligand (mercaptopropionic acid) functionalized GNPs by using both molecular dynamics simulation and experimental approach.[50] Importantly, none of the above-mentioned studies determined the orientation-dependent biological activity of cyt *c*. Therefore, we envisaged that for redox-active and

therapeutically important proteins such as cyt *c*, the orientation of heme moiety with respect to NP surface could play an important role in determining its activity.

To the best of our knowledge, no studies have appraised the ability of cyt *c* to instigate apoptosis when modulating its conformation and orientation on the surface of NPs. Therefore, the aim of this work was to tailor the surface chemistry of the GNPs to modulate the orientation and conformation of cyt *c*. Subsequently, we wanted to establish the effect of these structural and orientation changes on the bioactivity of cyt *c*. In order to do this, we have used GNP-cyt *c* nanoconjugates to analyze and relate the orientation of cyt *c* to its apoptotic activity. We have shown that electrostatic interactions between GNPs with different surface charge can induce different orientation of bound cyt *c* (**Figure 1**a). We have further detailed the changes in the cyt *c* secondary and tertiary structures caused by the charged ligands on GNPs (**Figure 1**b). Changes in the redox kinetics of cyt *c* arising from different orientations of the protein on GNPs were examined by electrochemical measurements (**Figure 1**c). Finally, we have assessed the effect of different orientation and change in cyt *c* structure on its apoptotic and peroxidase activity (**Figure 1**d). Based on the obtained results, we propose a general guideline that both protein structure and orientation on the surface of NPs should be considered, assessed and accounted when modulating biological activity.

2. Experimental Section

2.1. Materials: All the reagents were of analytical grade and were used as supplied without further purification unless specified. Citrate-capped spherical gold nanoparticles of size 125 nm were purchased from NanopartzTM, USA. Phosphate buffer saline (PBS, 10 mM), Horse heart cytochrome *c*, Thiol-PEG-Amine (MW = 2,000 Da), Trypsin, Bradford reagent and Guaiacol were purchased from Sigma-Aldrich, UK. Thiol-PEG-Acid and Thiol-PEG-Hydroxyl (MW = 2,000 Da) were purchased from Nanocs, USA. Caspase-3 assay kit (Colorimetric) was purchased from Abcam, Cambridge, UK. CellEventTM Caspase-3/7 Green detection reagent was bought from Invitrogen, ThermoFisher Scientific, UK.

2.2. Surface functionalization of gold nanoparticles: Cytochrome *c* (cyt *c*) was electrostatically adsorbed on gold nanoparticles (GNPs) using a two-step procedure. In the first step, GNPs were functionalized with a hetero-bifunctional PEG to obtain water soluble GNPs. Briefly, 10 mL of SH-PEG-COOH or SH-PEG-NH_2 or SH-PEG-OH (500 μM) solution in water was added to 10 mL citrate-capped GNPs (50 μg/mL). The solution was stirred overnight at room temperature. Later, the GNPs were centrifuged at 2500 rpm for 20 min and washed 4 times to obtain PEGylated GNPs named as GNP.COOH, GNP.NH_2 and GNP.OH. In the second step, 5 mL of cyt c was added to 5 mL PEGylated GNPs (GNP.COOH, GNP.NH_2 and GNP.OH) and the solution was stirred at room temperature for 24 h. Various concentrations of cyt c (100, 150, and 200 μM) were used to optimize its binding on PEGylated GNPs. Finally, the GNPs were centrifuged at 2500 rpm for 20 min and washed 4 times with water to obtain GNP.COOH.cyt *c*, GNP.NH_2.cyt *c*, and GNP.OH.cyt *c*.

2.3. Characterization

2.3.1. Transmission Electron Microscopy (TEM): Size and morphology of the GNPs was analyzed using a transmission electron microscope (JEOL 2000 FX TEM) operating at 200 kV accelerating voltage. TEM samples were prepared by dropping 15μL of GNPs on a carbon-coated copper grid (400 Mesh, Agar Scientific), the samples were allowed to sit on the grid for at least 3 h before imaging. Histogram of particle size distribution was obtained by analyzing 100 different nanoparticles of each sample.

2.3.2. Dynamic Light Scattering and Zeta Potential: The hydrodynamic diameter and Zeta potential of the GNPs were recorded using a Malvern Zetasizer Nano-ZS ((Malvern Instruments, UK).

2.3.3. UV-Vis Absorption and Circular Dichroism Spectroscopy: UV–Vis absorption spectra were recorded on a CARY 50 Bio Spectrophotometer (Varian). Far and near UV CD spectra were recorded at 20 ºC on a Chirascan CD spectrophotometer (Applied Photophysics) equipped with a temperature control unit TC125 (Quantum Northwest). All the samples and cyt *c* were dispersed in 10 mM PBS at pH 7.4. Three spectra were taken for

each sample and averaged. A quartz cuvette with an optical pathlength of 1 cm was used for all the UV-Vis and CD measurements.

2.3.4. X-ray Photoelectron Spectroscopy: Samples were analyzed using the Kratos AXIS ULTRA with a monochromatic Al kα X-ray source (1486.6eV) operated at 10 mA emission current and 12 kV anode potential (120 W) Spectra were acquired with the Kratos VISION II software. A charge neutralizer filament was used to prevent surface charging. Hybrid –slot mode was used measuring a sample area of approximately 300 × 700 μm. Three repeats of each sample with three different areas were performed. A wide scan at low resolution (Binding energy range 1400 eV to - 5 eV, with pass energy 80 eV, step 0.5 eV, sweep time 20 minutes) was used to estimate the total atomic % of the detected elements. High-resolution spectra at pass energy 20 eV, a step of 0.1 eV, and sweep times of 10 minutes each were also acquired for photoelectron peaks from the detected elements and these were used to model the chemical composition. The spectra were charge corrected to the C 1s peak (adventitious carbon or a known polymer CH_2 or CH_3 peak) set to 285 eV. The amount of cyt *c* on the surface of GNPs was determined by analyzing the atomic percentage of nitrogen (N 1s signal). For GNP.NH_2.cyt *c* samples, where Nitrogen (N) can also be detected to its presence in the GNP.NH_2, normalization with respect to both N and Au (atomic percentage) before and after cyt *c* binding was performed and Equation 1 was used to calculate the N_{norm}**[51]**.

$$\mathrm{N_{norm}} = \mathrm{N_p} - \mathrm{N_b}\left(\mathrm{Au_p} - \mathrm{Au_b}\right) \quad (1)$$

In Equation 1, N_b and Au_b are the calculated atomic percentage of N and Au, respectively, from the GNP.NH_2 samples i.e. before cyt *c* binding. Np and Au_p are the measured atomic percentage of N and Au, respectively, from the GNP.NH_2.cyt *c* samples.

2.3.5. Time of flight-Secondary Ion Mass Spectrometry (ToF-SIMS): For ToF-SIMS analysis, samples were drop casted onto IPA-wiped microscopy glass slides and dried in vacuum. ToF-SIMS analysis of positively and negatively charged secondary ions was carried out using a TOF.SIMS IV system from ION-TOF GmbH (Münster, Germany). For each sample, spectra were acquired using a 25 keV Bi^{3+} primary ion beam operated in the high current bunched mode delivering 0.3 pA and raster scanned 30 times over a 100 x 100 μm^2 area,

which kept the total dose under the static limit of 1012 ions/cm^2. A low-energy (20 eV) electron flood gun was employed to neutralize charge build-up. The ToF analyzer was set with 200 µs cycle time, resulting in a mass range between 0 and 3492 mass units. To account for variability, 6 spectra were acquired at different regions of each sample and near the center of the formed films. Control spectra of pure gold nanoparticles and clean glass substrate were also measured.

2.3.6. Electrochemical Studies: The analyses were conducted using a Metrohm Autolab M204 potentiostat and a three-electrode system within a Faraday cage (Princeton Applied Research). This consisted of a platinum wire counter electrode, an Ag/AgCl reference electrode (both from ALS Co. Ltd.) and an indium tin oxide (ITO, Delta Technologies Ltd.) working electrode. To construct the working electrode ITO coated glass was cut to approximately 10 mm × 20 mm; this was washed briefly with acetone and water, dried with argon gas and assembled into an electrochemical cell with an exposed working area of 38.48 mm^2. A new ITO working electrode was used for every sample tested. GNPs were dispersed in PBS to a final working concentration of 25 µg/mL (determined by UV-Vis). Cyclic voltammetry (CV) was conducted between 0.4 V and - 0.2 V at varying scan rates between 50 $mV.s^{-1}$ and 2 $V.s^{-1}$. Repetitive consecutive CVs were conducted at a fixed scan rate of 100 $mV.s^{-1}$. Control CVs were conducted with unmodified gold nanoparticles using PBS as the supporting electrolyte.

2.4. Proteolytic Degradation Assay: The assay was performed using the protocol reported earlier.[52] In a typical experiment, 1 mL of 25 µg/mL cyt c bound GNPs were incubated with 4 mg of trypsin for 1, 4, 8 and 24 h at 37 ºC. The degradation of cyt *c* was determined by monitoring the absorbance at 409 nm.

***2.5.* Cell Culture:** Malignant Glioblastoma cell line U251 were purchased from ATCC, USA and cultured in DMEM (Gibco) supplemented with 10% fetal bovine serum (FBS) and 1% penicillin/streptomycin. Cells were maintained at 37 °C in an incubator with humidified atmosphere, containing 5% CO_2.

2.6. Cellular uptake analysis: For cellular uptake analysis, 0.5×10^5 U251 cells were seeded on 6-well plate and incubated at 37 °C for 24 h. After 24 h, the culture medium was

replaced with fresh medium containing 25 µg/mL GNP functionalized with/ without cyt *c* and incubated for 1 and 4 h. After each incubation period the media was removed, and cells were washed three times with PBS to remove unbound/loosely bound GNPs. Cells were trypsinized and 50µL of cell suspension was used for trypan blue cell viability assay. The remaining cell suspension was centrifuged at 200 × g for 5 min. The obtained pellet was digested overnight with 5% aquaregia. Later the solutions were diluted with milliQ water to reach the final concentration of acid to 2% and taken for ICP-MS analysis (iCAPQ Thermo Fischer). The number of GNPs inside each cell was determined using the method reported earlier.**[53]**

2.7. Colorimetric Caspase-3 assay: For caspase-3 detection, two different approaches were studied. In the first approach the cells were first lysed to extract the cytosol, followed by GNP treatment to induce apoptosis and finally caspase-3 detection. While in the second approach, treatment with GNPs was given to the cells, followed by cytosol extraction and caspase-3 detection. In a typical experiment, 0.5×10^5 U251 cells were seeded on 6-well plate and incubated at 37°C for 24 h. Next, the culture medium was replaced with fresh medium containing 25 µg/mL GNPs functionalized with/ without cyt *c* and incubated for 1 and 4 h. Afterwards, cells were trypsinized and 1×10^6 cells were counted and resuspended in the 50 µL of chilled lysis buffer (supplied with the caspase-3 assay kit) and incubated in ice for 10 minutes. Later, the cells were centrifuged at 10,000 × g for 1 minute and the supernatant (cytosol) was transferred to a fresh tube. The protein content in the cytosolic extract was determined using the Bradford assay. For the second approach, the fresh cytosol (extracted using the protocol discussed above) was incubated with 25 µg/mL GNPs functionalized with/without cyt *c* and 2 µM free cyt *c* for 1 and 4 h. Finally, Caspase-3 assay was performed following the manufacturer's protocol in a 96-well plate. A total of 50 µL of 2X reaction buffer (containing 10 mM DTT) was added to 50 µL of each sample (in triplicate), followed by addition of 5 µL of the 4 mM DEVD-p-NA substrate. The reaction was incubated at 37 ºC for 90 min and the absorbance of the sample was read at 400 nm on a Tecan microplate reader. A sample without any treatment with GNPs or cyt *c* was taken as control. Background reading from 50

µL cytosol incubated with 50 µL reaction buffer was subtracted from both test and control samples. The experiments were repeated three times using triplicates.

2.8. Fluorescent Caspase-3/7 assay: 0.5×10^5 U251 cells were seeded on a 35 mm glass-bottom dish (ThermoFisher SCIENTIFIC) and incubated at 37°C for 24 h. After 24 h, the culture medium was replaced with fresh medium containing 25 µg/mL GNPs functionalized with/ without cyt *c* and incubated for 4 h. After 4 h, media containing GNPs was removed and cells were washed three times with PBS. Next, the cells were incubated with 8 µM CellEventTM Caspase 3-7 green detection reagent in PBS containing 5% FBS for 30 min at 37 ºC. Afterwards, the cells were preserved with 3.7% formaldehyde for 15 min and subsequently washed with PBS. Later the cells were treated with DAPI for 5 min at RT under dark and washed again with PBS. Finally, the cells were immersed in PBS and imaged using Zeiss Elyra confocal microscope at 20x objective using the filter settings of Alexa Fluor 488 dye. The green fluorescent intensity values were normalized to the total number of cells per field and expressed as corrected total cell fluorescence (CTCF) obtained by Equation 2:

Corrected total cell fluorescence = Integrated density - (area of selected cell × Mean fluorescence of background signal) (2)

2.9. WST-8 metabolic activity assay: Biocompatibility of GNPs and cyt *c* bound GNPs was studied using WST-8 assay. A total of 1×10^4 U251 cells were incubated on 96 well plates 24 h prior experiment. During the next step, the culture media was replaced with medium containing GNPs (12.5 or 25 µg/mL) and incubated for 4 h. Next, media was replaced with 10% WST-8 in complete DMEM and incubated for an hour before reading the absorbance at 450 nm in a Tecan microplate reader. Culture media and 3% Triton X-100 were taken as negative and positive control respectively. Values are presented relative to negative controls.

2.10. Peroxidase activity: To determine the peroxidase activity, the oxidation of Guaiacol (2-methoxyhenol) by H_2O_2 in the presence/ absence of native cyt *c* and GNPs functionalized with cyt *c* was recorded. GNP-cyt *c* conjugates (1 mL) in various concentrations (6.25, 12.5, and 25µg/mL) was added to 2.5 µM Guaiacol (1 mL) and finally 250 µM H_2O_2 was

added and incubated for 5 min and absorbance was taken at 470 nm. PBS (1 mL), 2.5 μM Guaiacol (1 mL) and 250 μM H_2O_2 (1 mL) was taken as control.

2.11. Statistical analysis: All the statistical analyses were performed using GraphPad Prism v8.2.1 software (GraphPad Software, Inc). All the data is expressed as mean ± S.D., unless specified. For responses that were affected by two variables, a 2-way ANOVA with a Tukey post-test was used. Results are expressed as mean ± SEM and a $P \leq 0.05$ was considered significant.

3. Results and Discussions

3.1. Synthesis and characterization of GNP.cyt c nanoconjugates: GNP-protein conjugates have become a popular choice in nanomedicine and sensing applications because of the physicochemical properties of GNPs, such as ease of surface modification, surface plasmon resonance (SPR), stability and biocompatibility.**[54-58]** Therefore, we set out to customize the surface chemistry of GNPs where we hypothesized that this would aid in modulating cyt *c* orientation and conformation. The synthesis of GNP.cyt *c* conjugates was accomplished by first generating three different sets of GNPs coated with either cationic, anionic, or neutral ligands of identical molecular weight (2000 Da) under physiological conditions for cyt *c* binding. The citrate-capped GNPs were named GNP.COOH, GNP.NH_2, and GNP.OH upon functionalization with thiol-PEG-carboxylic acid, thiol-PEG-amine, and thiol-PEG-hydroxyl, respectively. Later, cyt *c* was adsorbed on these PEGylated GNPs upon incubation for 24 h, which was followed by multiple washing to remove any unbound protein. The obtained GNP.cyt *c* conjugates were named GNP.COOH.cyt *c*, GNP.NH_2.cyt *c*, and GNP.OH.cyt *c* (**Figure 1**a).

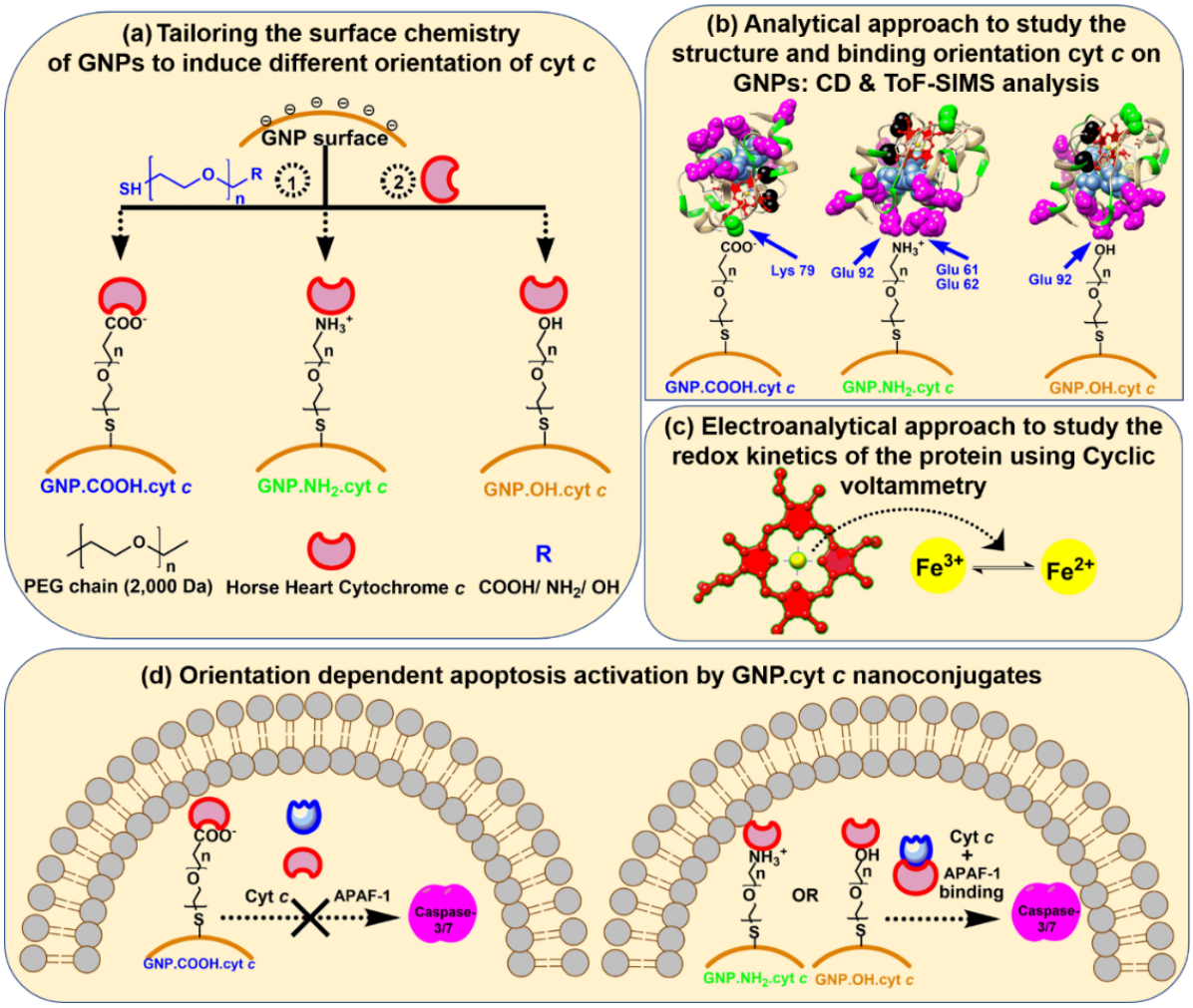

Figure 1. Schematic representation of the experimental approach followed to investigate the orientation dependent apoptotic activity of cyt *c* bound GNPs. (a) Surface functionalization of citrate-capped GNPs with anionic, cationic and neutral ligands to modulate the orientation of cyt *c*. (b) Analytical approach to identify the structure and orientation of cyt *c* on GNPs. Proposed model for the adsorption orientation and interaction site of cyt *c* on GNPs with three different ligands. The crystal structure of horse heart cyt *c* was obtained from PDB (1 HRC) and University of California, San Francisco (UCSF) Chimera (version 1.14 rc) was used to label amino acid residues and heme ring. In cyt *c* structure – red: heme/porphyrin ring; black: cysteine (Cys); magenta: glutamic acid (Glu); blue: leucine (Leu); green: lysine (Lys); and yellow: Iron (Fe). (c) Electroanalytical approach to study the redox kinetics of cyt *c* bound to GNPs. (d) *In vitro* cell culture studies to analyze the capability of cyt *c* bound GNPs to activate Caspase-3/7.

Cyt *c* consists of positively charged Lysine (Lys) residues that are distributed across the protein and negatively charged glutamic acid residues on the other side near to the heme moiety in the protein structure.[59-61] We expected that cyt *c* would have a different orientation on GNPs functionalized with different ligands resulting from electrostatic interactions. TEM measurements revealed that the mean diameter of different GNP.cyt *c* conjugates is between 130-133 nm (**Figure 2**a-c). The UV-Vis absorption spectrum of free cyt *c* exhibited the Soret band at λ_{max} = 409 nm and another peak centered at 525 nm corresponding to the Q band. The presence of this single Q band has been attributed to the oxidized form of cyt *c*.[62] The absorption spectrum of citrate-capped GNPs showed a characteristic surface plasmon resonance (SPR) peak at λ_{max} = 569 nm. After cyt *c* binding all the samples showed peaks corresponding to the Soret band of cyt *c* at λ_{max} = 409 nm and a slightly red-shifted SPR band at λ_{max} = 572 nm (**Figure 2**d). By using the UV-Vis absorption spectra and extinction coefficient of PEGylated GNPs and cyt *c*, an estimation of the concentration and number of cyt *c* molecules attached to single GNP was derived using Beer Lambert law (**Table S1**). The detailed calculation (**Figure S1-S3)** gave an upper estimate of the number of cyt *c* molecules on a single GNP.COOH.cyt *c*, GNP.NH_2.cyt *c*, and GNP.OH.cyt *c* nanoparticle of $\sim 1.57 \times 10^5$, $\sim 1.56 \times 10^5$, $\sim 1.55 \times 10^5$, respectively, when GNP.COOH, GNP.NH_2, and GNP.OH samples were incubated with cyt *c* at a concentration of either 100, 150, or 150 μM, respectively. Considering, cyt c (d =3.1 nm; r = 1.5 nm) as a circle, its area = ~ 7.07 nm^2 and PEGylated GNP (average r = 67.5 nm) as a sphere, its area = ~ 57255 nm^2. Therefore, in a monolayer model a maximum of 8098 cyt *c* can be accommodated on each PEGylated GNP. Based on our calculation there are on average $\sim 1.56 \times 10^5$ cyt c molecules adsorbed on different GNP composite. This value of no. of cyt *c* on each GNP suggests multilayer adsorption (n = ~19-20 layers) of cyt *c* on GNPs, which could have been facilitated by the pH of the solution as well as electrostatic interaction between different protein layers.[63] Nevertheless, our data indicates that a similar number of cyt *c* /GNP (average = $\sim 1.56 \times 10^5$) was achieved, thereby, fulfilling one of the most important pre-requisites i.e. similar protein adsorption, for evaluating the biological activity of different protein-nanoparticle conjugates. Dynamic light scattering

(DLS) analyses revealed an increase in the hydrodynamic diameter of GNPs after surface modification with the ligand and cyt *c* (**Figure 2**e). The zeta potential (ζ) data indicates that GNPs with different surface charges were obtained after functionalization with different heterobifunctional PEG ligands (**Figure 2**f). The ζ values of ligands-functionalized GNPs changed significantly to positive after cyt *c* binding, which could be a result of an overall positive charge of cyt *c*.[64] Furthermore, GNP.COOH.cyt *c*, GNP.NH_2.cyt *c*, and GNP.OH.cyt *c* displayed a polydispersity index (PDI) of 0.13, 0.11, and 0.09, indicating that the samples are very homogeneous (**Figure S4**) and again indicate multilayer formation of the cyt *c* on GNPs.

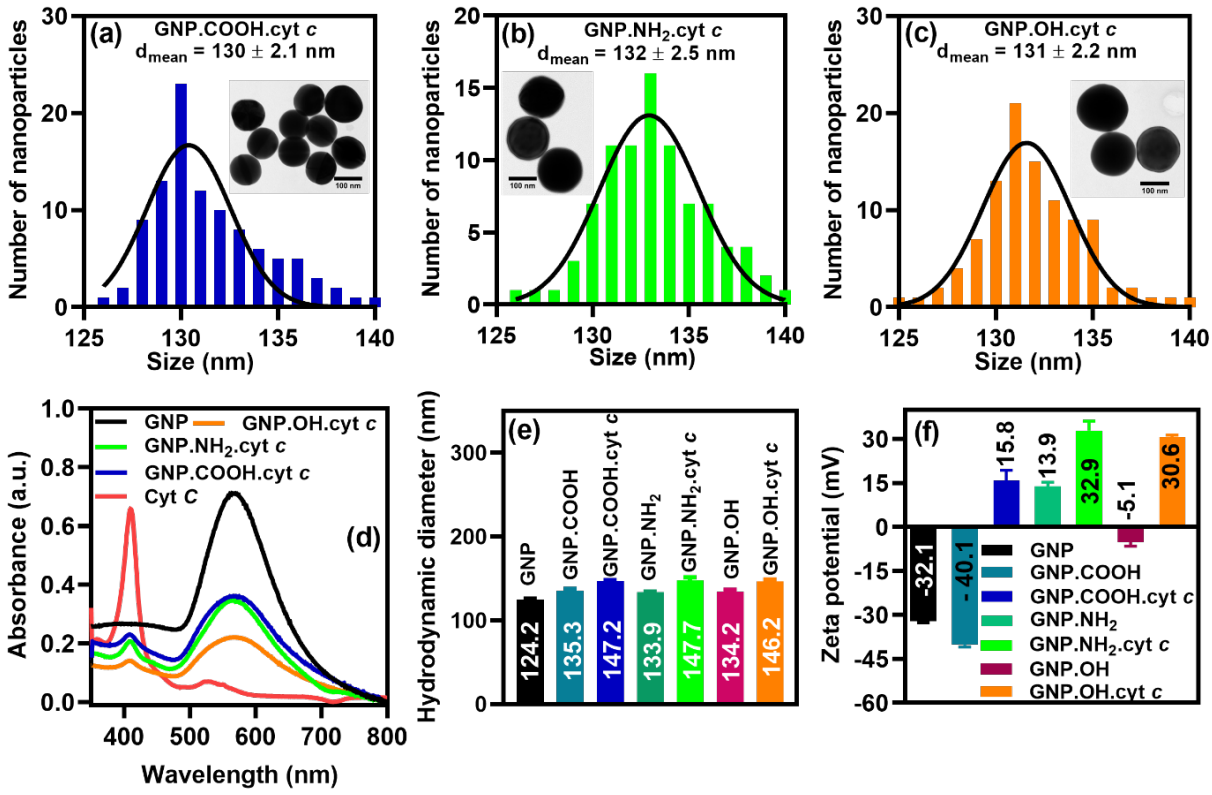

Figure 2. Physicochemical characterization of cyt *c* bound GNPs using three different ligands. (a, b and c) Histogram of the particle size distribution of cyt *c* bound GNPs using cationic (GNP.COOH), anionic (GNP.NH_2) and neutral ligand (GNP.OH), respectively. Inset shows the representative TEM image. (d) UV-Vis absorption spectrum; (e) Hydrodynamic diameter analyzed using DLS and (f) Zeta potential of unmodified citrate-capped gold nanoparticles

(GNPs) and surface-modified GNPs. The error bars represent the S.E.M of the average value obtained after measurements from three different preparation of GNPs.

XPS analyses was further conducted to confirm if a similar concentration of cyt *c* is bound to GNPs with different ligands using the atomic percentage (at. %) of N. All the samples exhibit similar amounts of nitrogen, 7.3 ± 0.5, 7.2 ± 0.3, 7.1 ± 0.3 at % for GNP.COOH.cyt *c* (100 µM), GNP.NH_2.cyt *c* (150 µM), and GNP.OH.cyt *c* (150 µM) nanoparticle, respectively **(Table 1)**. Therefore, we only studied the biological activity of the samples which were produced when GNP.COOH, GNP.NH_2, and GNP.OH samples were incubated with cyt *c* at a concentration of either 100, 150, or 150 µM, respectively. The XPS quantification analyses is consistent with UV-Vis data, thus confirming that similar number of cyt c/GNP were obtained.

Table S2. Summary of elemental composition (in atomic percentage) for GNPs as determined by XPS analysis before and after cyt *c* binding. Error bars represent standard deviations of atomic percentage obtained from three analysis spots on three different samples.

Sample name	Au (4f)	C (1s)	O (1s)	S (2p)	N (1s)
Citrate-capped GNP	67.1 ± 0.8	48.6 ± 0.4	4.3 ± 0.6	-	-
GNP.COOH	52.2 ± 4.8	38.6 ± 2.8	5.9 ± 0.2	3.3 ± 0.2	-
GNP.NH_2	45.1 ± 3.7	44.5 ± 2.1	6.9 ± 0.3	4.1 ± 0.4	1.8 ± 0.2
GNP.OH	53.2 ± 3.1	36.8 ± 1.7	6.6 ± 0.1	3.4 ± 0.2	-
GNP.COOH.cyt *c* (100 µM)	49.3 ± 1.5	32.5 ± 0.9	6.7 ± 0.3	4.2 ± 0.3	7.3 ± 0.5
GNP.NH_2.cyt *c* (150 µM)	51.4 ± 2.1	31.3 ± 2.4	6.1 ± 0.4	4 ± 0.2	8.1 ± 0.3 7.2 ± 0.3 (N_{norm})
GNP.OH.cyt *c* (150 µM)	48.7 ± 2.6	33.1 ± 1.1	7.2 ± 0.6	3.9 ± 0.4	7.1 ± 0.3

3.2. Analytical approach to determine the structure, conformation and orientation of cyt c on GNPs: Circular dichroism (CD) spectroscopy was utilized to investigate the structure of cyt c bound to GNPs. In a UV CD spectrum (200 - 260 nm), molecular ellipticity at 208 and 222 nm represent the α helical content and catalytical activity of the protein**.** [65] In this work, all the

samples including native cyt c showed two double minima at 208 and 222 nm. A slight loss and improvement in the helicity of cyt c bound to GNP.COOH and GNP.OH, respectively (**Figure 3**a) was observed. However, all the samples showed similar pattern and molecular ellipticity to that of native cyt *c*. Therefore, these results suggest that cyt *c* retains its native secondary structure on GNPs with different ligands.

The UV CD spectra of native cyt *c* in the range 260 - 360 nm showed (**Figure 3**b) two minima at 282 and 288 nm attributed to the tertiary structure of Tryptophan (Trp) residues.[66] In GNP.COOH.cyt *c,* the blue shift in one of the minima to 278 nm indicates that the tertiary structure is perturbed compared with the native cyt *c*. On the other hand, GNP.NH_2.cyt *c* and GNP.OH.cyt *c* samples showed almost identical Trp minima as native cyt *c*, indicating that the tertiary structure of cyt *c* remains unchanged.

Further insight on the tertiary structure of the amino acid residues near to the heme ring was obtained by monitoring the Soret region (360 – 450 nm) of the CD spectra. The Soret CD spectra of native cyt *c,* GNP.NH_2.cyt *c* and GNP.OH.cyt *c* (**Figure 3**c) showed almost identical spectra with two positive maxima (406 and 397 nm) and one negative minimum (419 nm) indicating no structural perturbation around the heme moiety. However, for the GNP.COOH.cyt *c* samples, the negative minimum red-shifted to 423 nm and an increase in molecular ellipticity of the positive peaks were observed, indicating slight perturbation in cyt *c* structure in the vicinity of heme ring. Overall, the CD analysis revealed that cyt *c* retains its secondary structure in all the samples irrespective of the charge of the ligands. However, the tertiary structure of cyt *c* is distorted in the GNPs functionalized with an anionic ligand, which could be a result of a strong electrostatic interaction between the carboxylate groups and positively charged amino acid residues adjacent to the heme ring.

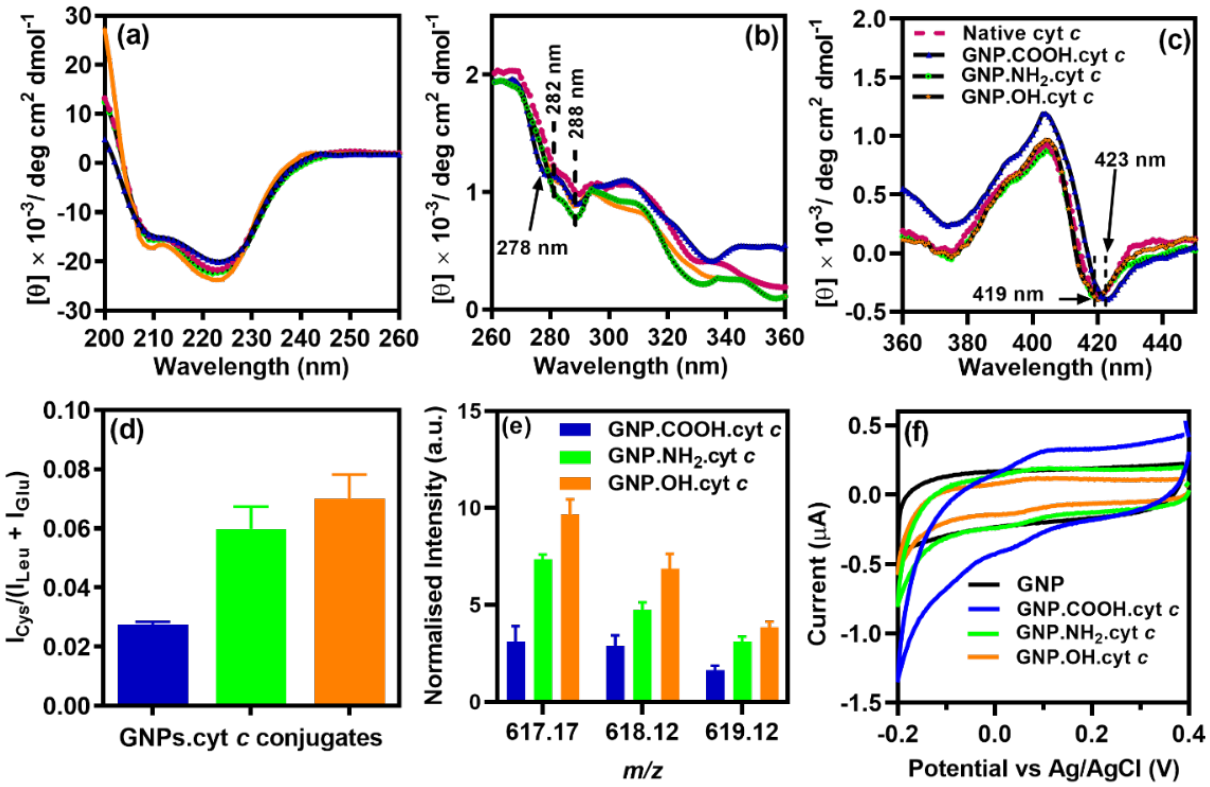

Figure 3. Structure and orientation of cyt *c* bound to GNPs. (a) Far-UV CD; (b) near-UV CD; and (c) Soret CD spectrum of free native cyt *c* and cyt *c* bound to GNPs in 10 mM PBS (pH = 7.4). All samples with identical concentration (25 μg/mL) were used for spectrum acquisition. Three spectra of each sample were collected and averaged. (d) ToF-SIMS peak intensity ratio, represented as the sum of intensities from cysteine/glumatic acid + leucine for cyt *c* bound GNP samples. (e) ToF-SIMS peak intensities for cyt *c* heme ring fragment. Error bars represent the standard deviation across six different analysis spots. (f) Comparative cyclic voltammograms (CVs) of GNPs with different orientations of cyt *c*. A scan rate of 100 $mV.s^{-1}$. Redox potentials measured using an Indium tin oxide (ITO) working electrode with different samples dispersed in PBS. Similar colors have been used in (a)-(c) and (d)-(e) to represent the samples.

ToF-SIMS was used to probe the orientation of cyt *c* when bound to GNPs using different ligands. The approach followed takes advantage of the extremely high surface sensitivity of ToF-SIMS to correlate changes in protein orientation to changes in the secondary ion intensity related to cysteine residues (I_{cys}: $C_2H_6NS^+$ - 76.015 u) that exist next to the heme

moiety, and glutamic acid (I_{Glu}: $C_6H_6NO^+$ - 84.053 u and $C_4H_8NO_2^+$ - 102.046 u) and leucine (I_{Leu}: $C_5H_{12}N^+$ - 86.09 u) rich region at the opposite end of the heme region. The average diameter of cyt c is ~3.1 nm and ToF-SIMS probes only the first few nanometers (3-4 nm) in depth of a sample, thus can only predict the orientation of cyt *c* that appear at the outermost/exposed layer in a multilayer adsorption model. Therefore, the ratio $R = I_{Cys} / (I_{Leu} + I_{Glu})$ for cyt *c* bound GNP samples with three different ligands can be used as a probe to determine cyt *c* orientation as previously established by Baio et al.[67] The analysis revealed nearly 50% difference in R values between GNP.COOH.cyt *c* and GNP.OH.cyt *c* or GNP.NH_2.cyt *c* (**Figure 3**d), where a similar ratio has been reported earlier in an approach previously established for flat gold surfaces.[67] The obtained data provides significant evidences that suggest the different orientation of cyt *c* on GNPs with the different ligands. Therefore, we hypothesized that in GNP.COOH.cyt *c* samples the Cys residues must be located near to the ligand-protein interface, thus explaining the lower value of R and vice-versa for Glu or Leu residues (protein-medium interface). On the other hand, the higher R values for the GNP.OH.cyt *c* and GNP.NH_2.cyt *c* samples indicate that the Glu and Leu residues are near to the ligand surface. To support this hypothesis, we analyzed the secondary ion intensity from the heme moiety consisting an iron-porphyrin fragments ($C_{34}H_{33}N_4O_4Fe^+$ - 617.186 u, 618.12 u and 619.12 u) (**Figure 3**e and **Figure S**5). The obtained results agree with the observed differences in R values, indicating that the position of heme group changes because of different cyt *c* orientation induced by different ligands and accepts the hypothesis. Additionally, the ToF-SIMS data suggest the possibility of oriented growth of cyt *c* multilayer on GNPs, which has precedent.[68] Nevertheless, ToF-SIMS data reported in this work suggest the average orientation cyt *c* (only the top layer of multilayer adsorption) on GNPs i.e. the most preferred orientation or the orientation that is adopted by cyt *c* on a greater number of GNPs. [50]

By carefully analyzing the crystal structure of cyt *c* (Horse heart; PDB entry 1 HRC), CD and ToF-SIMS data, we propose the adsorption orientation of cyt *c* bound to GNPs using

different ligands (**Figure 1**b). In GNP.COOH.cyt *c* sample, cyt *c* adopts an orientation wherein the heme ring is buried near to the protein-ligand interface with positively charged Lys_{79} residues interacting with carboxylate groups of the ligand through electrostatic interaction. Such an orientation results in Cys residues near to the carboxylic group of the ligand thus causing the disruption of thioester linkage and thus justify the observed perturbation in the tertiary structure of cyt *c* (observed in CD spectrum) on GNP.COOH.cyt *c* samples. Similar orientation of cyt *c* was reported by Lin et al. on 11-mercaptoundecanoic acid-modified gold electrodes.[43] In GNP.NH_2.cyt *c* and GNP.OH.cyt *c* samples, cyt *c* adopts an orientation opposite to GNP.COOH.cyt *c* samples, with the heme cleft exposed to the top of the surface and near to the protein-medium interface. This orientation results in negatively charged Glu_{61}, Glu_{62}, and Glu_{92} residues near to the amine groups and Glu_{92} residues near to the hydroxyl group of the ligands suggesting that the nature of interaction could be ionic or hydrogen bonding.

We also established the effect of tuning the molecular conformation and orientation of cyt *c* on its redox properties. We performed cyclic voltammetry (CV) analyses of the different GNP.cyt *c* conjugates at 100 $mV.s^{-1}$. We also conducted a scan rate study over the range of 50 $mV.s^{-1}$ to 2 $V.s^{-1}$ (**Figure S6** a-c). A redox couple was observed for the cyt *c* bound GNP samples that was not present in the unmodified GNP control (**Figure 3**f). The presence of these redox peaks at ~ 0.09 V (oxidation peak) and ~ 0.039 V (reduction peak) has been attributed to the redox nature of Fe center embedded in the heme ring of cyt *c*.[69] Notably, the observed redox couple is only because of cyt *c* bound to GNPs, as the peaks originating from protonation and deprotonation of the surface reactive groups (carboxylic, amine, hydroxyl and thiols) does not coincide with the redox peaks reported in this work.[70] Peak separation recorded at the 100 $mV.s^{-1}$ scan rate was 69 mV, 76 mV and 65 mV for the GNP.COOH.cyt *c*, GNP.NH_2.cyt *c* and GNP.OH.cyt *c* samples, respectively. On analyzing the scan rate study, a proportional relationship was seen when plotting peak current vs scan rate (**Figure S6** d-f). These important observations are indicative of a surface-bound electrochemical process and supports our

assertion of the proposed surface modification and suggests that the surface chemistry is stable. This is further supported by the fact that there is no significant difference in peak reducing current measured after 100 consecutive scan rates (**Figure S6** g-i); if cyt *c* was dissociating due from ligands, the peak current associated with cyt *c* would become smaller. It is worth mentioning that consecutive scan rate studies have been used to prove the affinity and stability of cyt *c* and other molecules adsorbed on the surface of nanoparticles or surfaces.[71-73] Therefore, our analyses show that the functionalized nanoparticles are stable and cyt c is bound tightly enough to the surface bound ligands. To study the redox state of heme Fe center in cyt *c* we calculated the formal electrode potential, where we observed values of 126 mV, 112 mV and 116 mV for GNP.COOH.cyt *c*, GNP.NH_2.cyt *c* and GNP.OH.cyt *c*, respectively; this observed difference in the values of formal electrode potential indicates that the ratio of Fe oxidation states in the heme ring differs in cyt *c* bound GNPs samples. This is important as the redox ratio of Fe within the cyt *c* has been linked to its peroxidase activity which can possibly affect its apoptotic induction capability.[74]

3.3. Orientation dependent apoptotic and peroxidase activity of GNP.cyt c nanoconjugates: Encouraged by our findings that cyt *c* adopts different orientations on GNPs and also due the fact that only the outermost layer of the protein over the nanoparticles defines the cell–nanoparticle interactions and biological activity of the nanoparticle-protein composite,[75] we wanted to establish an understanding of conformation and orientation effects on apoptotic activity of GNP.cyt *c* conjugates. However, considering the possibility of cyt *c* degradation by proteases under *in vitro* conditions, we first conducted a trypsin-based degradation assay,[76] to examine the degradation of cyt *c* bound to GNPs. We observed similar degradation kinetics for all the samples upon incubation with 4 mg/mL of trypsin (**Figure 4**a). Approximately 10% degradation of cyt *c* was observed at 1 and 4 h, however, as expected, after 8 h, there was a significant increase in the degradation of cyt *c* bound to GNPs. Nevertheless, for the cell-based experiments, we chose 1 and 4 h as the optimum time period to study the biological response of these GNPs because all the samples showed almost

identical degradation of cyt *c.* As our data indicated that the surface chemistry of nanoparticles is similar between the GNPs until 4h and the ligand differences is not impacting on the biological stability of the cyt *c*.

Next, we assessed the capability of cyt *c* bound GNPs to induce apoptosis using a colorimetric assay that detects the activity of Caspase-3, which is upregulated during apoptosis. However, it has been reported earlier that cyt *c* is a membrane-impermeable protein [77] and it is thus critical to analyze the ability of cyt *c* bound GNPs to activate Caspase-3 in a cell-free system. Therefore, we first analyzed the Caspase-3 activation in freshly extracted cytosol from U251 malignant brain tumor cells upon incubation with native cyt *c* and GNP.cyt *c* conjugates for 1 and 4 h. As shown in **Figure 4**b, we observe a significantly higher (*p*-value < 0.0001) Caspase-3 activation in cytosol incubated with native cyt *c,* GNP.NH_2.cyt *c* or GNP.OH.cyt *c* compared to GNP.COOH.cyt *c*. The observed difference in Caspase-3 activation between the different GNP.cyt *c* conjugates could result only from the difference in their capability to interact with Apoptotic protease activating factor 1 (APAF-1), induced by the different orientation of cyt *c* on GNPs.

Before testing this hypothesis *in vitro*, that the orientation of cyt *c* governs its apoptotic activity, we studied the cellular association of cyt *c* bound GNPs with U251 cells using Inductively Coupled Plasma Mass Spectrometry (ICP-MS). ICP-MS analysis revealed that there was no significant difference in the association of cyt *c* bound to GNPs using different ligands with U251 cells at 1 and 4 h (**Figure 4**c). Interestingly, we found that cyt *c* bound GNPs showed significantly less association compared to GNPs functionalized with ligands. This observed difference in the cellular association could be caused by the membrane-impermeability of cyt *c*. Nevertheless, the obtained data suggest similar level of association between the cells and different GNP.cyt *c* conjugates. The results obtained in a cell-free system were validated by performing Caspase and metabolic assays *in vitro*. The Caspase-3 activation in U251 cells upon incubation with GNPs show that GNP.NH_2.cyt *c* and GNP.OH.cyt *c* have the highest Caspase-3 activation at 1 and 4 h (*p*-value < 0.05 vs GNP.COOH.cyt *c*),

while native cyt *c* and ligands functionalized GNPs showed negligible Caspase-3 activation (**Figure 4**d).

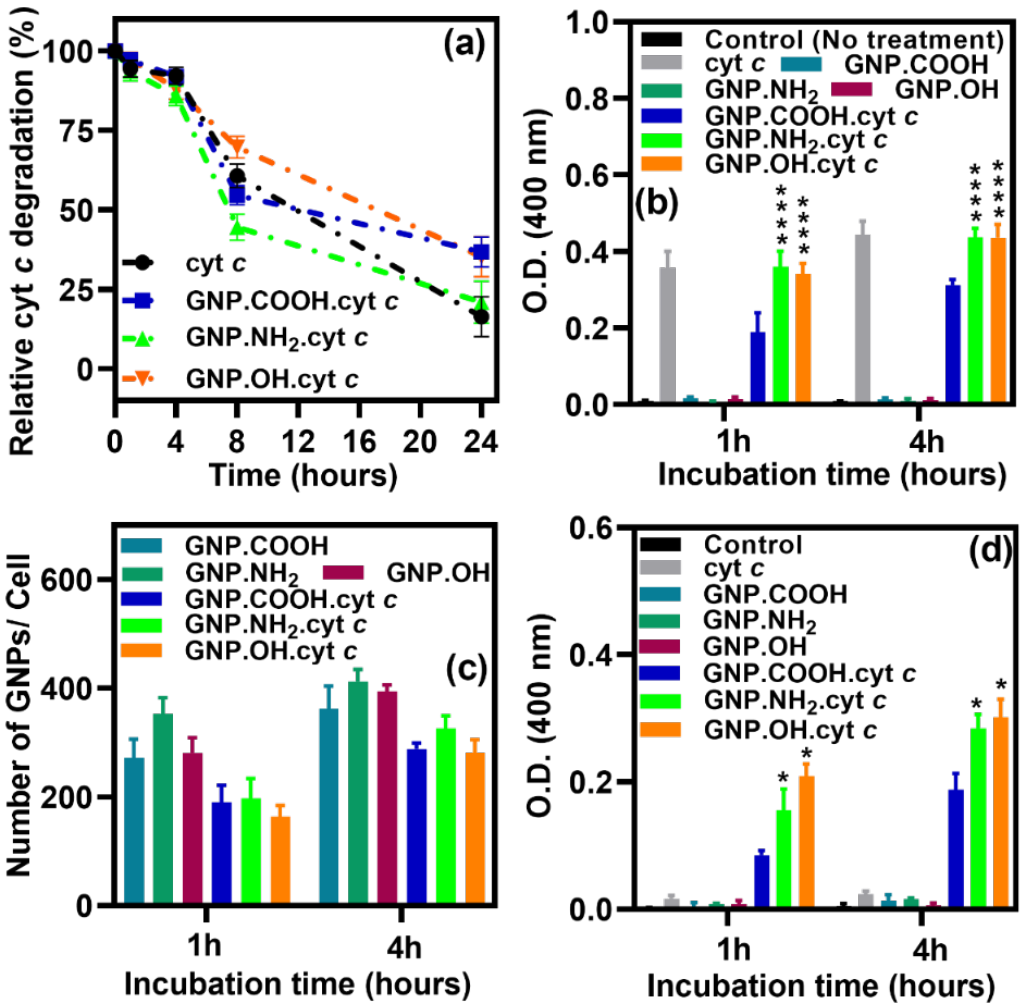

Figure 4. Orientation dependent apoptotic activity of cyt *c* bound GNPs. (a) Degradation kinetics of free and GNPs bound cyt *c* upon incubation with trypsin at 37º. (b) Cell-free colorimetric Caspase-3 activity assay to determine the capability of different GNP.cyt *c* conjugates to induce apoptosis. (c) ICP-MS analysis to determine the association of GNPs with U251 glioblastoma cells, the data is expressed as the number of GNPs per cell. (d) *In vitro* Caspase-3 assay in U251 cells incubated with cyt *c* bound GNPs for 1 and 4 h. All the experiments were performed in triplicates and repeated for atleast 2-3 times. Results are expressed as mean ± S.D. *P < 0.05; ****P < 0.0001 vs GNP.COOH.cyt *c*, obtained using 2-way ANOVA with a Tukey post-test.

We further confirmed these results by conducting a fluorescence-based Caspase-3/7 assay. **Figure 5** a-c show the confocal microscopy images of U251 cells treated with cyt *c* bound GNP samples. The presence of green color arises from the activation of Caspase-3/7 was ~50% higher in cells treated with GNP.NH_2.cyt *c* or GNP.OH.cyt *c* compared to GNP.COOH.cyt *c* (**Figure 5**d). On the other hand, no significant difference in Caspase-3 activation was found between GNP.NH_2.cyt *c* and GNP.OH.cyt *c* samples. Moreover, the GNPs functionalized only with ligands (no cyt *c*) and free native cyt *c* do not elicit any Caspase activation (**Figure S7** a-e). These *in vitro* results are consistent with our studies in a cell-free system, thereby supporting our hypothesis. Therefore, based on the obtained results, we believe that the difference in Caspase-3 activation by GNPs is because of the orientation of cyt *c* induced by the surface charge of the ligands. Furthermore, it is worth mentioning that the observed effect is not due to different levels of association between GNP.cyt *c* conjugates and the cells, otherwise we would have observed a significant difference in the cellular association of different GNP.cyt *c* conjugates and conversely in the apoptosis inducing capability of GNP.cyt *c* conjugates in a cell-free system. The cationic and neutral ligands permit cyt *c* to adopt an orientation in which the heme cleft is exposed and accessible for establishing interaction with the WD-40 domain of APAF-1, thus initiating the apoptosis cascade eventually leading to Caspase-3 activation.**[78-80]**

The successful Caspase-3 activation induced by cyt *c* bound GNPs allowed us to further study their effect on the metabolic activity of U251 cells. No significant change in the metabolic viability of U251 cells is observed upon incubation with different GNP.cyt *c* conjugates at lower concentration (12.5 µg/mL). A 20% decrease in cell viability was observed after 4 h of incubation with different GNP.cyt *c* conjugates at a higher concentration (25 µg/mL). Statistical analysis revealed that the observed decrease in the viability is significant (GNP.COOH.cyt *c* *vs* GNP.NH_2.cyt *c* or GNP.OH.cyt *c*; *p*-value < 0.01) (**Figure S8**).

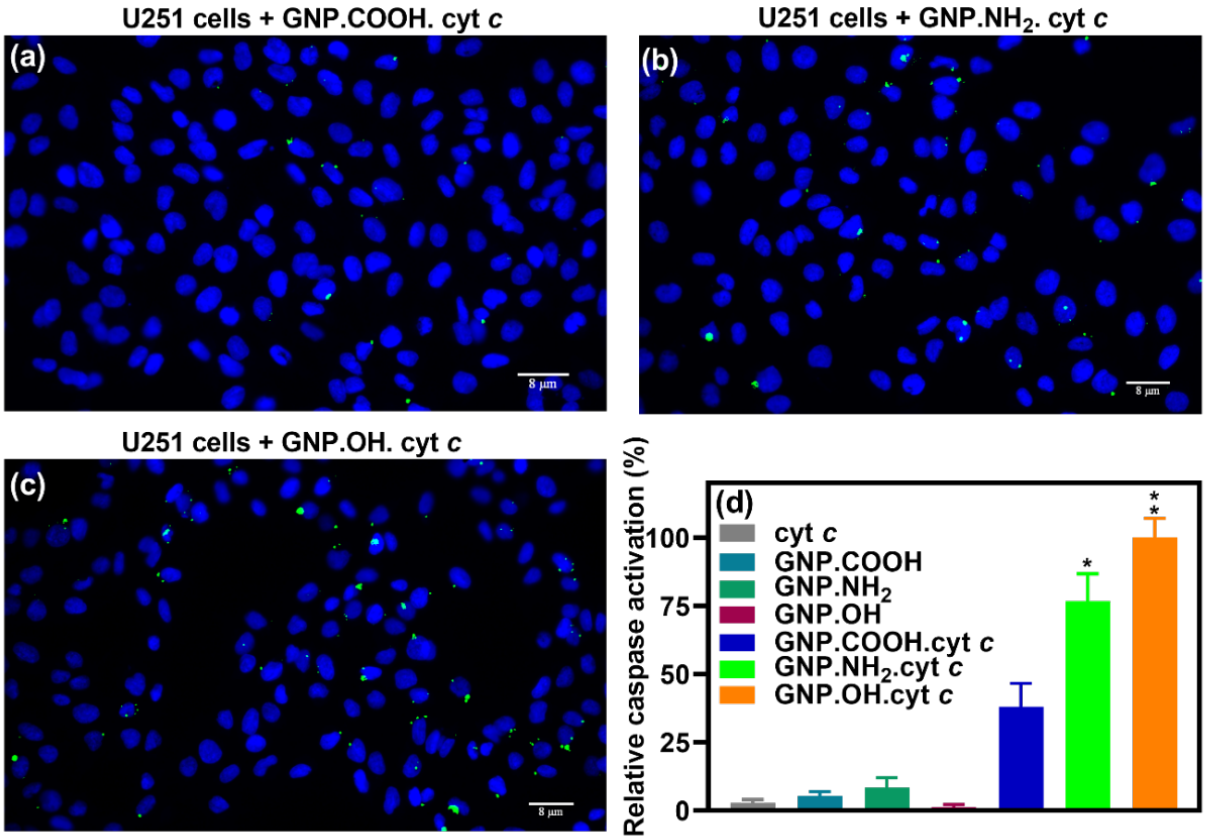

Figure 5. Fluorescent Caspase activity assay. (a-c) Confocal microscopy images of U251 cells incubated with different GNP. cyt *c* conjugates for 4 h, cells with green fluorescence are Caspase-3/7 positive cells. (d) Corrected total cell fluorescence as a function of relative Caspase activation induced by cyt c bound GNPs in U251 cells. All the values were normalized with fluorescent intensity obtained with GNP.OH.cyt *c* samples. Error bars represent the SEM of fluorescent intensity of at least 25 different cells. *P < 0.05; **P < 0.01 vs GNP.COOH.cyt *c*, obtained using 2-way ANOVA with a Bonferroni post-test

Finally, to confirm whether the structural perturbation observed in the CD spectra of GNP.COOH.cyt *c* sample is affecting its apoptotic activity, we tested the peroxidase activity of GNP.cyt *c* conjugates. Since, it has been previously reported that the perturbation in the tertiary structure of cyt *c* causes increased access to the heme ring that leads to an enhancement in peroxidase activity,**[74, 81]** a higher peroxidase activity of GNP.COOH.cyt *c* would be expected compared to GNP.NH_2.cyt *c* and GNP.OH.cyt *c*. Guaiacol, an oxidation indicator was used to monitor the peroxidase activity of cyt *c* bound GNPs in the presence of H_2O_2. After incubating the different GNP samples at various concentrations with the substrate, we

observed that GNP.NH_2.cyt *c* and GNP.OH.cyt *c* samples have significantly higher peroxidase activity compared to GNP.COOH.cyt *c* sample (**Figure 6**). While there was no significant difference in between GNP.NH_2.cyt *c* and GNP.OH.cyt *c* samples. This data indicates that even after perturbation of cyt *c* structure in GNP.COOH.cyt *c* samples, the heme ring is not easily accessible to the substrate for oxidation; this can only be the case when the heme is protected deep inside the protein structure. While in GNP.NH_2.cyt *c* and GNP.OH.cyt *c* samples, the heme ring is more accessible and exposed to the external environment (as suggested by ToF-SIMS data), which contribute to the higher peroxidase activity. Moreover, we show GNPs modified with the ligand only had no significant peroxidase activity.

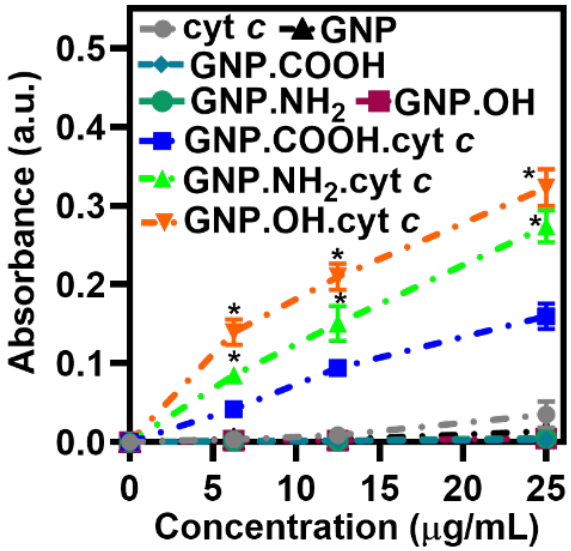

Figure 6. Orientation dependent Peroxidase activity of cyt *c* bound GNPs using three different ligands as a function of their concentration. Experiment was performed in quadruplicates and results are expressed as mean ± S.D. *P < 0.05 vs GNP.COOH.cyt *c*, obtained using 2-way ANOVA with a Tukey post-test.

These results show that orientation of proteins on nanoparticles can be tailored by tuning the surface chemistry on nanoparticles. This work further highlights that both protein structure and orientation play a vital role in determining the activity of cyt c. Furthermore, ToF-SIMS can be employed to identify proteins orientation on nano-structured surfaces. And since the approach is based on the fact that different protein orientations will have different relative amounts of specific amino acids closer to the top surface, it can be applied to other proteins

given 3D structure, amino acid sequence and position of active sites are known. This work opens up an opportunity for researchers to analyse the orientation-dependent activity of other proteins which are of great importance in the field of diagnostics, sensing and therapeutics

4. Conclusions

In summary, we have demonstrated that the surface charge of the ligand on GNPs alters the conformation and orientation of cyt *c*. Anionic ligands cause perturbation in the tertiary structure of cyt *c*, while the structure was preserved on the cationic and neutral ligands. The adsorption of cyt *c* on anionic and cationic or neutral ligand is facilitated by the interaction with Lys and Glu residues, respectively. We have further identified that the apoptotic and peroxidase activity of cyt *c,* when bound to GNPs, is dependent on the position of the heme ring with respect to its structure. A specific orientation with exposed heme ring favored apoptotic activity, because of easier access of heme edge for interaction with the apoptosis initiating protein (APAF-1). In contrast, suppressed apoptotic activity is observed for the opposite orientation with the heme ring protected. This study shows that by changing the surface charge of the ligand on the NP surface, the activity of cyt *c* can be modulated to achieve the desired response. We anticipate that these novel findings will facilitate the design and application of new sensors and protein-based nanomedicine for a broad range of diseases.

Supplementary information (SI)

Additional information as noted in the text including quantification of number of cyt c molecules bound to each GNPs using UV-Vis spectroscopy **(Figure S1-S3 & Table S1)**. Dynamic light scattering data of different GNP.cyt *c* conjugates **(Figure S4)**. TOF-SIMS intensity spectra of iron-porphyrin fragments (**Figure S5**). Cyclic volatmograms of scan rate and redox kinetics of different GNP.cyt *c* nanoconjuages (**Figure S6**). Confocal microscopy images of ligand functionalized GNPs and other controls for fluorescent Caspase 3-7 activity assay (**Figure S7**). WST-8 metabolic activity assay (**Figure S8**).

Acknowledgements

This work is supported by the Engineering and Physical Sciences Research Council (EPSRC) Grant number EP/R004072/1, EU ERDF (FEDER) funds and Spanish government grant TEC2017-85059-C3-2-R. L.P.G. thanks the University of Nottingham for a Anne McLaren Research Fellowship. D.B.A. thanks the EPSRC for funding [EP/M005178/1]. Dr. Scott Young, Dr. Liz Bailey and Dr. Saul Vazquez-Reina are thanked for their assistance with ICP-MS analysis. Dr. Mario Samperi is thanked for assistance with circular dichroism analysis. We thank the Nanoscale and Microscale Research Centre (nmRC) for providing access to instrumentation. Dr. Nigel Neate and Dr. Craig Stoppiello are thanked for assistance on TEM and XPS analysis, respectively.

Authors contribution

Akhil Jain: Conceptualization & Methodology, Writing- Original draft preparation, Visualization, Investigation (Synthesis and characterization of surface-functionalized gold nanoparticles, Circular Dichroism analysis, Electrochemical measurements, Cell culture studies, Peroxidase activity), Writing- Reviewing and Editing, Formal analysis. **Gustavo F. Trindade:** Investigation (ToF-SIMS measurements & analysis), Writing- Reviewing and Editing. **Jacqueline M. Hicks:** Investigation (Electrochemical measurements & analysis). **Jordan C. Potts:** Investigation (Synthesis and characterization of surface-functionalized gold nanoparticles). **Ruman Rahman:** Resources and Writing- Reviewing and Editing. **Richard J. M. Hague:** Resources and Writing- Reviewing and Editing. **David B. Amabilino:** Conceptualization & Methodology, Validation, Writing- Reviewing and Editing. **Lluïsa Pérez-García:** Resources, Conceptualization & Methodology, Validation, Writing- Reviewing and Editing. **Frankie J. Rawson:** Conceptualization & Methodology, Validation, Writing- Original draft preparation, Writing- Reviewing and Editing, Supervision, Funding Acquisition.

Conflict of interest

The authors declare no conflict of interest.

References

[1] P.M. Mendes, Cellular nanotechnology: making biological interfaces smarter, Chem. Soc. Rev. 42(24) (2013) 9207-9218.

[2] F. Rawson, C. Yeung, S. Jackson, P. Mendes, Tailoring 3D single-walled carbon nanotubes anchored to indium tin oxide for natural cellular uptake and intracellular sensing, Nano lett.13(1) (2012) 1-8.

[3] P. Zhang, L. Chen, T. Xu, H. Liu, X. Liu, J. Meng, G. Yang, L. Jiang, S. Wang, Programmable fractal nanostructured interfaces for specific recognition and electrochemical release of cancer cells, Adv. Mater. 25(26) (2013) 3566-3570.

[4] A.J. Sivaram, A. Wardiana, C.B. Howard, S.M. Mahler, K.J. Thurecht, Recent advances in the generation of antibody–nanomaterial conjugates, Adv. Healthcare Mater. 7(1) (2018) 1700607.

[5] S. Rana, Y.-C. Yeh, V.M. Rotello, Engineering the nanoparticle–protein interface: applications and possibilities, Curr. opin. chem. biol. 14(6) (2010) 828-834.

[6] R. Solaro, F. Chiellini, A. Battisti, Targeted delivery of protein drugs by nanocarriers, Materials 3(3) (2010) 1928-1980.

[7] C.D. Spicer, C. Jumeaux, B. Gupta, M.M. Stevens, Peptide and protein nanoparticle conjugates: versatile platforms for biomedical applications, Chem. Soc. Rev. 47(10) (2018) 3574-3620.

[8] A. Kapur, F. Aldeek, X. Ji, M. Safi, W. Wang, A. Del Cid, O. Steinbock, H. Mattoussi, Self-Assembled Gold Nanoparticle–Fluorescent Protein Conjugates as Platforms for Sensing Thiolate Compounds via Modulation of Energy Transfer Quenching, Bioconjugate chem. 28(2) (2017) 678-687.

[9] M. De, S. Rana, H. Akpinar, O.R. Miranda, R.R. Arvizo, U.H. Bunz, V.M. Rotello, Sensing of proteins in human serum using conjugates of nanoparticles and green fluorescent protein, Nature chem. 1(6) (2009) 461.

[10] J.R. Ashton, E.B. Gottlin, E.F. Patz, Jr., J.L. West, C.T. Badea, A comparative analysis of EGFR-targeting antibodies for gold nanoparticle CT imaging of lung cancer, PLoS One 13(11) (2018) e0206950.

[11] S. Mao, G. Lu, K. Yu, Z. Bo, J. Chen, Specific protein detection using thermally reduced graphene oxide sheet decorated with gold nanoparticle‐antibody conjugates, Adv. Mater. 22(32) (2010) 3521-3526.

[12] G.A. Pietersz, X. Wang, M.L. Yap, B. Lim, K. Peter, Therapeutic targeting in nanomedicine: the future lies in recombinant antibodies, Nanomedicine 12(15) (2017) 1873-1889.
[13] K. Ulbrich, K. Hola, V. Subr, A. Bakandritsos, J. Tucek, R. Zboril, Targeted drug delivery with polymers and magnetic nanoparticles: covalent and noncovalent approaches, release control, and clinical studies, Chem. rev. 116(9) (2016) 5338-5431.
[14] G.Y. Tonga, K. Saha, V.M. Rotello, 25th anniversary article: interfacing nanoparticles and biology: new strategies for biomedicine, Adv. Mater. 26(3) (2014) 359-370.
[15] K. Kalimuthu, B.-C. Lubin, A. Bazylevich, G. Gellerman, O. Shpilberg, G. Luboshits, M.A. Firer, Gold nanoparticles stabilize peptide-drug-conjugates for sustained targeted drug delivery to cancer cells, J. nanobiotechnol. 16(1) (2018) 34.
[16] L. Cheng, L. Yang, F. Meng, Z. Zhong, Protein nanotherapeutics as an emerging modality for cancer therapy, Adv. Healthcare Mater. 7(20) (2018) 1800685.
[17] J. Cai, J. Yang, D. Jones, Mitochondrial control of apoptosis: the role of cytochrome c, BBA-Bioenergetics 1366(1-2) (1998) 139-149.
[18] M. Hüttemann, P. Pecina, M. Rainbolt, T.H. Sanderson, V.E. Kagan, L. Samavati, J.W. Doan, I. Lee, The multiple functions of cytochrome c and their regulation in life and death decisions of the mammalian cell: From respiration to apoptosis, Mitochondrion 11(3) (2011) 369-381.
[19] W.R. Fisher, H. Taniuchi, C.B. Anfinsen, On the role of heme in the formation of the structure of cytochrome c, J. Biol. Chem. 248(9) (1973) 3188-3195.
[20] G.C. Brown, V. Borutaite, Regulation of apoptosis by the redox state of cytochrome c, BBA-Bioenergetics 1777(7-8) (2008) 877-881.
[21] M. Saxena, Y. Delgado, R.K. Sharma, S. Sharma, S.L.P.D.L. Guzmán, A.D. Tinoco, K. Griebenow, Inducing cell death in vitro in cancer cells by targeted delivery of cytochrome c via a transferrin conjugate, PloS one 13(4) (2018) e0195542.
[22] A. Fu, R. Tang, J. Hardie, M.E. Farkas, V.M. Rotello, Promises and pitfalls of intracellular delivery of proteins, Bioconjugate chem. 25(9) (2014) 1602-1608.
[23] S. Papadopoulos, K.D. Jürgens, G. Gros, Protein diffusion in living skeletal muscle fibers: dependence on protein size, fiber type, and contraction, Biophysical j. 79(4) (2000) 2084-2094.
[24] I.I. Slowing, B.G. Trewyn, V.S.-Y. Lin, Mesoporous silica nanoparticles for intracellular delivery of membrane-impermeable proteins, J. Am. Chem. Soc.129(28) (2007) 8845-8849.

[25] S.K. Kim, M.B. Foote, L. Huang, The targeted intracellular delivery of cytochrome C protein to tumors using lipid-apolipoprotein nanoparticles, Biomaterials 33(15) (2012) 3959-3966.
[26] W. Al-Shakarchi, A. Alsuraifi, M. Abed, M. Abdullah, A. Richardson, A. Curtis, C. Hoskins, Combined Effect of Anticancer Agents and Cytochrome C Decorated Hybrid Nanoparticles for Liver Cancer Therapy, Pharmaceutics 10(2) (2018) 48.
[27] A.A. Vertegel, R.W. Siegel, J.S. Dordick, Silica nanoparticle size influences the structure and enzymatic activity of adsorbed lysozyme, Langmuir 20(16) (2004) 6800-6807.
[28] P. Roach, D. Farrar, C.C. Perry, Surface tailoring for controlled protein adsorption: effect of topography at the nanometer scale and chemistry, J. Am. Chem. Soc.128(12) (2006) 3939-3945.
[29] M.E. Aubin-Tam, K. Hamad-Schifferli, Gold nanoparticle-cytochrome C complexes: the effect of nanoparticle ligand charge on protein structure, Langmuir 21(26) (2005) 12080-4.
[30] L. Shang, L. Yang, J. Seiter, M. Heinle, G. Brenner‐Weiss, D. Gerthsen, G.U. Nienhaus, Nanoparticles interacting with proteins and cells: a systematic study of protein surface charge effects, Adv. Mater. Interfaces 1(2) (2014) 1300079.
[31] H. Bayraktar, C.-C. You, V.M. Rotello, M.J. Knapp, Facial control of nanoparticle binding to cytochrome c, J. Am. Chem. Soc. 129(10) (2007) 2732-2733.
[32] M.E. Aubin-Tam, W. Hwang, K. Hamad-Schifferli, Site-directed nanoparticle labeling of cytochrome c, Proc Natl Acad Sci U S A 106(11) (2009) 4095-100.
[33] W. Shang, J.H. Nuffer, V.A. Muñiz‐Papandrea, W. Colón, R.W. Siegel, J.S. Dordick, Cytochrome c on silica nanoparticles: influence of nanoparticle size on protein structure, stability, and activity, Small 5(4) (2009) 470-476.
[34] S. Maiti, K. Das, S. Dutta, P.K. Das, Striking Improvement in Peroxidase Activity of Cytochrome c by Modulating Hydrophobicity of Surface‐Functionalized Gold Nanoparticles within Cationic Reverse Micelles, Chem. Eur. J. 18(47) (2012) 15021-15030.
[35] E. Matysiak-Brynda, B. Wagner, M. Bystrzejewski, I.P. Grudzinski, A.M. Nowicka, The importance of antibody orientation in the electrochemical detection of ferritin, Biosens. Bioelectron 109 (2018) 83-89.
[36] L.M. Herda, D.R. Hristov, M.C. Lo Giudice, E. Polo, K.A. Dawson, Mapping of molecular structure of the nanoscale surface in bionanoparticles, J. Am. Chem. Soc.139(1) (2016) 111-114.

[37] F. Liu, L. Wang, H. Wang, L. Yuan, J. Li, J.L. Brash, H. Chen, Modulating the activity of protein conjugated to gold nanoparticles by site-directed orientation and surface density of bound protein, ACS Appl. Mater. Interfaces 7(6) (2015) 3717-3724.
[38] D. Wasserberg, J. Cabanas-Danés, J. Prangsma, S. O'Mahony, P.-A. Cazade, E. Tromp, C. Blum, D. Thompson, J. Huskens, V. Subramaniam, Controlling protein surface orientation by strategic placement of oligo-histidine tags, ACS nano 11(9) (2017) 9068-9083.
[39] S. Mazzucchelli, M. Colombo, P. Verderio, E. Rozek, F. Andreata, E. Galbiati, P. Tortora, F. Corsi, D. Prosperi, Orientation‐Controlled Conjugation of Haloalkane Dehalogenase Fused Homing Peptides to Multifunctional Nanoparticles for the Specific Recognition of Cancer Cells, Angew. Chem. Int. Ed. Engl. 52(11) (2013) 3121-3125.
[40] K.W. Yong, D. Yuen, M.Z. Chen, C.J. Porter, A.P. Johnston, Pointing in the Right Direction: Controlling the Orientation of Proteins on Nanoparticles Improves Targeting Efficiency, Nano lett.19(3) (2019) 1827-1831.
[41] P. Zhang, L. Zhang, Z. Qin, S. Hua, Z. Guo, C. Chu, H. Lin, Y. Zhang, W. Li, X. Zhang, Genetically Engineered Liposome‐like Nanovesicles as Active Targeted Transport Platform, Adv. Mater. 30(7) (2018) 1705350.
[42] J. Xu, E.F. Bowden, Determination of the orientation of adsorbed cytochrome c on carboxyalkanethiol self-assembled monolayers by in situ differential modification, J. Am. Chem. Soc.128(21) (2006) 6813-6822.
[43] S. Lin, X. Jiang, L. Wang, G. Li, L. Guo, Adsorption orientation of horse heart cytochrome c on a bare gold electrode hampers its electron transfer, J. Phy. Chem. C 116(1) (2011) 637-642.
[44] K. Ataka, J. Heberle, Functional vibrational spectroscopy of a cytochrome c monolayer: SEIDAS probes the interaction with different surface-modified electrodes, J Am Chem Soc 126(30) (2004) 9445-57.
[45] C.E. Caesar, E.K. Esbjörner, P. Lincoln, B. Nordén, Assigning membrane binding geometry of cytochrome C by polarized light spectroscopy, Biophysical j. 96(8) (2009) 3399-3411.
[46] J.M. Pachence, S. Amador, G. Maniara, J. Vanderkooi, P. Dutton, J. Blasie, Orientation and lateral mobility of cytochrome c on the surface of ultrathin lipid multilayer films, Biophysical j. 58(2) (1990) 379-389.
[47] A. Tronin, A.M. Edwards, W.W. Wright, J.M. Vanderkooi, J.K. Blasie, Orientation distributions for cytochrome c on polar and nonpolar interfaces by total internal reflection fluorescence, Biophysical j. 82(2) (2002) 996-1003.

[48] J. Zhou, J. Zheng, S. Jiang, Molecular simulation studies of the orientation and conformation of cytochrome c adsorbed on self-assembled monolayers, J. Phy. Chem. B 108(45) (2004) 17418-17424.
[49] G. Di Palma, A.M. Kotowska, L.R. Hart, D.J. Scurr, F.J. Rawson, S. Tommasone, P.M. Mendes, Reversible, high-affinity surface capturing of proteins directed by supramolecular assembly, ACS Appl. Mater. Interfaces 11(9) (2019) 8937-8944.
[50] E.J. Tollefson, C.R. Allen, G. Chong, X. Zhang, N.D. Rozanov, A. Bautista, J.J. Cerda, J.A. Pedersen, C.J. Murphy, E.E. Carlson, Preferential binding of cytochrome c to anionic ligand-coated gold nanoparticles: A complementary computational and experimental approach, ACS nano 13(6) (2019) 6856-6866.
[51] R. Michel, S. Pasche, M. Textor, D.G. Castner, Influence of PEG architecture on protein adsorption and conformation, Langmuir 21(26) (2005) 12327-12332.
[52] J. Méndez, M. Morales Cruz, Y. Delgado, C.M. Figueroa, E.A. Orellano, M. Morales, A. Monteagudo, K. Griebenow, Delivery of chemically glycosylated cytochrome c immobilized in mesoporous silica nanoparticles induces apoptosis in HeLa cancer cells, Mol. pharmaceutics 11(1) (2013) 102-111.
[53] P. Sanjuan-Alberte, A. Jain, A.J. Shaw, S.A. Abayzeed, R.F. Domínguez, M.E. Alea-Reyes, M. Clark, M.R. Alexander, R.J. Hague, L.s. Pérez-García, Wireless Nanobioelectronics for Electrical Intracellular Sensing, ACS Applied Nano Materials (2019).
[54] Y.-C. Yeh, B. Creran, V.M. Rotello, Gold nanoparticles: preparation, properties, and applications in bionanotechnology, Nanoscale 4(6) (2012) 1871-1880.
[55] N.R. Jana, J.Y. Ying, Synthesis of functionalized Au nanoparticles for protein detection, Adv. Mater. 20(3) (2008) 430-434.
[56] K.C. Kwon, E. Jo, Y.W. Kwon, B. Lee, J.H. Ryu, E.J. Lee, K. Kim, J. Lee, Superparamagnetic gold nanoparticles synthesized on protein particle scaffolds for cancer theragnosis, Adv. Mater. 29(38) (2017) 1701146.
[57] X. Cheng, R. Sun, L. Yin, Z. Chai, H. Shi, M. Gao, Light‐Triggered Assembly of Gold Nanoparticles for Photothermal Therapy and Photoacoustic Imaging of Tumors In Vivo, Adv. Mater. 29(6) (2017) 1604894.
[58] W. Chen, S. Zhang, Y. Yu, H. Zhang, Q. He, Structural‐engineering rationales of gold nanoparticles for cancer theranostics, Adv. Mater. 28(39) (2016) 8567-8585.
[59] P.L. Edmiston, J.E. Lee, S.-S. Cheng, S.S. Saavedra, Molecular orientation distributions in protein films. 1. Cytochrome c adsorbed to substrates of variable surface chemistry, J. Am. Chem. Soc.119(3) (1997) 560-570.

[60] L. Banci, I. Bertini, H.B. Gray, C. Luchinat, T. Reddig, A. Rosato, P. Turano, Solution structure of oxidized horse heart cytochrome c, Biochemistry 36(32) (1997) 9867-9877.
[61] G.W. Bushnell, G.V. Louie, G.D. Brayer, High-resolution three-dimensional structure of horse heart cytochrome c, Journal of molecular biology 214(2) (1990) 585-595.
[62] S. Ferretti, S.-K. Lee, B.D. MacCraith, A.G. Oliva, D.J. Richardson, D.A. Russell, K.E. Sapsford, M. Vidal, Optical biosensing of nitrite ions using cytochrome cd1 nitrite reductase encapsulated in a sol–gel matrix, Analyst 125(11) (2000) 1993-1999.
[63] D.V. Sotnikov, A.N. Berlina, V.S. Ivanov, A.V. Zherdev, B.B. Dzantiev, Adsorption of proteins on gold nanoparticles: One or more layers?, Colloids and Surfaces B: Biointerfaces 173 (2019) 557-563.
[64] C. Kawai, F.M. Prado, G.L. Nunes, P. Di Mascio, A.M. Carmona-Ribeiro, I.L. Nantes, pH-dependent interaction of cytochrome c with mitochondrial mimetic membranes The role of an array of positively charged amino acids, Journal of Biological Chemistry 280(41) (2005) 34709-34717.
[65] N.J. Greenfield, Using circular dichroism spectra to estimate protein secondary structure, Nature protocols 1(6) (2006) 2876.
[66] S. Vinogradov, R. Zand, Circular dichroism studies: I. Cytochrome c, Archives of biochemistry and biophysics 125(3) (1968) 902-910.
[67] J.E. Baio, T. Weidner, D. Ramey, L. Pruzinsky, D.G. Castner, Probing the orientation of electrostatically immobilized cytochrome C by time of flight secondary ion mass spectrometry and sum frequency generation spectroscopy, Biointerphases 8(1) (2013) 18.
[68] H. Kawakubo, S. Isoda, K. Inatomi, Y. Hanazato, S. Ueyama, M. Maeda, Molecular orientation and photoelectric properties of molecular heterojunction using flavin-cytochrome c multilayers, [1990] Proceedings of the Twelfth Annual International Conference of the IEEE Engineering in Medicine and Biology Society, IEEE, 1990, pp. 1754-1755.
[69] A.K. Yagati, T. Lee, J. Min, J.-W. Choi, Electrochemical performance of gold nanoparticle–cytochrome c hybrid interface for H2O2 detection, Colloids Surf. B. Biointerfaces 92 (2012) 161-167.
[70] X. Chen, R. Ferrigno, J. Yang, G.M. Whitesides, Redox properties of cytochrome c adsorbed on self-assembled monolayers: a probe for protein conformation and orientation, Langmuir 18(18) (2002) 7009-7015.
[71] B. Dinesh, V. Mani, R. Saraswathi, S.-M. Chen, Direct electrochemistry of cytochrome c immobilized on a graphene oxide–carbon nanotube composite for picomolar detection of hydrogen peroxide, Rsc Advances 4(54) (2014) 28229-28237.

[72] D.D. Schlereth, Characterization of protein monolayers by surface plasmon resonance combined with cyclic voltammetry 'in situ', Journal of electroanalytical chemistry 464(2) (1999) 198-207.
[73] M.T. Ghafari, F. Varmaghani, B. Karimi, V. Khakyzadeh, Robust non-covalent and covalent anchored N, N, N′, N'-tetramethyl-p-phenylenediamine derivative on electrode surface via spontaneous physical immobilization and in situ generated aryldiazonium ion electro-grafting: implication for on-surface chemistry and electro-catalytic determinations, Analyst 145(2) (2020) 596-606.
[74] L. Tarpani, F. Bellezza, P. Sassi, M. Gambucci, A. Cipiciani, L. Latterini, New Insights into the Effects of Surface Functionalization on the Peroxidase Activity of Cytochrome c Adsorbed on Silica Nanoparticles, J. Phy. Chem. B 123(11) (2019) 2567-2575.
[75] I. Lynch, Are there generic mechanisms governing interactions between nanoparticles and cells? Epitope mapping the outer layer of the protein–material interface, Physica A: Statistical Mechanics and its Applications 373 (2007) 511-520.
[76] D.P. Reinhardt, R.N. Ono, L.Y. Sakai, Calcium stabilizes fibrillin-1 against proteolytic degradation, Journal of Biological Chemistry 272(2) (1997) 1231-1236.
[77] S. Santra, C. Kaittanis, J.M. Perez, Cytochrome C encapsulating theranostic nanoparticles: a novel bifunctional system for targeted delivery of therapeutic membrane-impermeable proteins to tumors and imaging of cancer therapy, Molecular pharmaceutics 7(4) (2010) 1209-1222.
[78] D.N. Shalaeva, D.V. Dibrova, M.Y. Galperin, A.Y. Mulkidjanian, Modeling of interaction between cytochrome c and the WD domains of Apaf-1: bifurcated salt bridges underlying apoptosome assembly, Biology direct 10(1) (2015) 29.
[79] L. Dorstyn, C.W. Akey, S. Kumar, New insights into apoptosome structure and function, Cell Death & Differentiation 25(7) (2018) 1194-1208.
[80] S. Yuan, M. Topf, T.F. Reubold, S. Eschenburg, C.W. Akey, Changes in Apaf-1 conformation that drive apoptosome assembly, Biochemistry 52(13) (2013) 2319-2327.
[81] P. Weinkam, J.r. Zimmermann, F.E. Romesberg, P.G. Wolynes, The folding energy landscape and free energy excitations of cytochrome c, Accounts of chemical research 43(5) (2010) 652-660.

Graphical Abstract

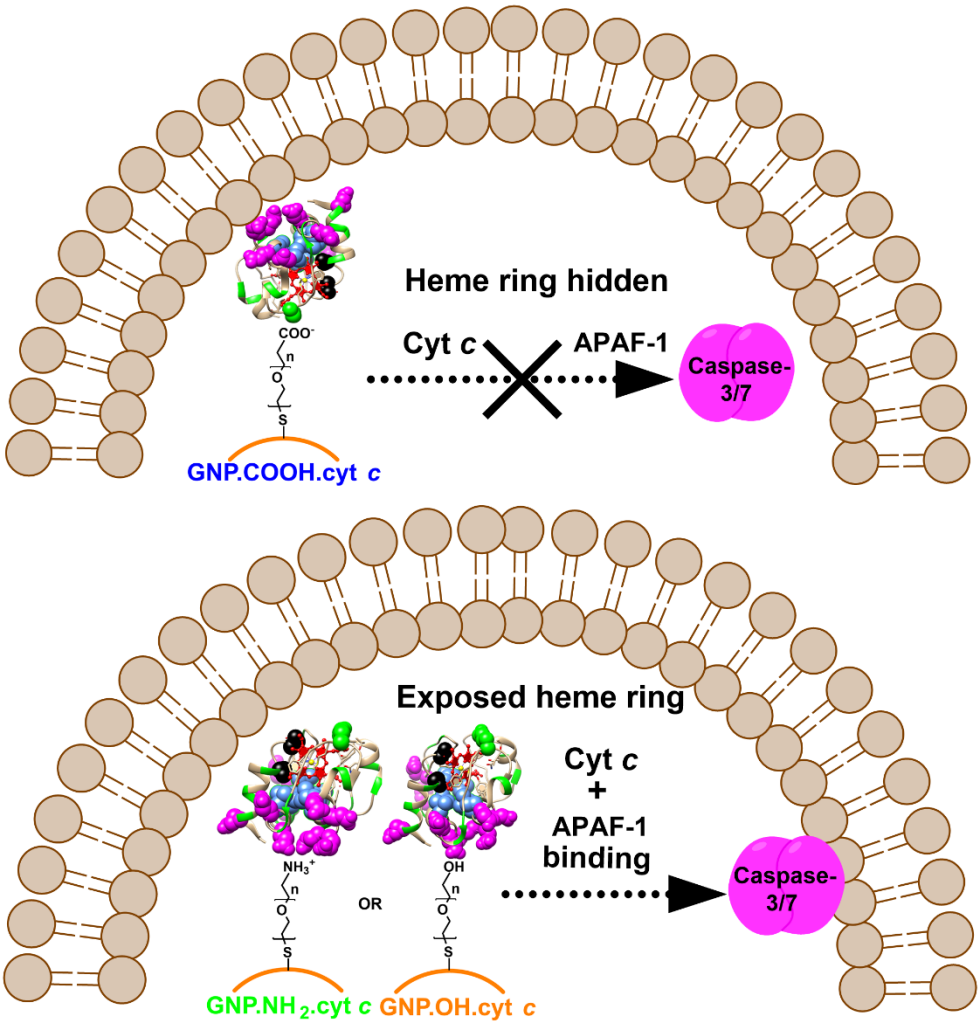
Heme ring hidden
Cyt c
APAF-1
Caspase-3/7
COO-
n
O
S
GNP.COOH.cyt c
Exposed heme ring
Cyt c
+
APAF-1
binding
Caspase-3/7
NH3+
OH
OR
GNP.NH2.cyt c
GNP.OH.cyt c